

THE INTERNATIONAL JOURNAL OF SCIENCE & TECHNOLEDGE

Macromolecular Azo Dye Complexes as Precursors to Metal Oxide Nanoparticles: Synthesis, Characterization, Biological Activity and Thermal Studies of Sulfadimidine Azo Dye Complexes

Aida L. El-Ansary

Faculty of Science, Department of Chemistry, Cairo University, Giza, Egypt

Omaima E. Sherif

Faculty of Science, Department of Chemistry, Cairo University, Giza, Egypt

Nora S. Abdel-Kader

Faculty of Science, Department of Chemistry, Cairo University, Giza, Egypt

Amira G. Sayed

Faculty of Science, Department of Chemistry, Cairo University, Giza, Egypt

Abstract:

Two azo dyes, L^1 and L^2 were synthesized from hydroxyl naphthoic acids and sulfadimidine drug. These azo dyes were characterized by elemental analyses, mass, IR and $^1\text{H-NMR}$ spectra. A series of Ni(II), Cu(II), Zn(II) and Pd(II) complexes were prepared with azo dyes, L^1 and L^2 . The mode of chelation of the complexes has been proposed in the light of many analytical tools such as elemental analyses, UV-Vis, IR, magnetic moment measurements, ESR and thermal studies. The measured molar conductance values indicate that the complexes are non-electrolytes. The thermal decomposition kinetics of the complexes of L^1 was estimated by Coats-Redfern equation. The azo dye L^1 complexes with Ni(II) and Cu(II) ions are thermally decomposed in solid state at 600 °C for 2 hours. Synthesized nanoparticles have been characterized by X-ray diffraction (XRD), Scanning electron microscope (SEM) and Fourier transform infrared spectroscopy (FTIR). The results show that NiO and CuO nanoparticles can be prepared using Ni(II)- L^1 and Cu(II)- L^1 complexes with high purity. The azo dyes and their complexes have been screened for their antibacterial activity against *Escherichia coli* as gram negative and *Staphylococcus aureus* as gram positive bacteria.

Keywords: sulfadimidine, azo dye complexes, thermal studies, nanoparticles, antibacterial

1. Introduction

Azo dyes are large class of synthetic organic dyes that contain nitrogen as the azo group $-\text{N}=\text{N}-$ as part of their molecular structures; more than half the commercial dyes belong to this class [1]. Azo compounds have intense colors due to their extensions of the delocalized aromatic π electron system being possible by the presence of the azo group [2].

Azo dyes have been widely used in various fields and have many applications in chemistry, pharmaceutical and radiochemical industry [3-7].

2-Hydroxy-1-naphthoic acid is a naphthalene compound with a weak fluorescence that is mainly used as an intermediate in the production of dyes and photosensitive materials [8]. Hydroxynaphthoic acid can adopt several different modes of bonding and forms stable chelates with different metal ions [9].

Sulfonamides were the first effective chemotherapeutic agents to be employed systematically for the prevention and cure of bacterial infections. Sulfa drugs kill bacteria by interfering with their metabolism. They were the "wonder drugs" before penicillin and are still used today. Sulfa drugs are bacteriostatic; i.e., they inhibit the growth and multiplication of bacteria but do not kill them. They act by interfering with the synthesis of folic acid [10]. Historically, medicinal inorganic chemistry is rich in metal- or metalloid-based drugs [11]. The field of bioinorganic chemistry, which deals with the study of the role of metal complexes in biological systems, has opened a new horizon for scientific research in coordination compounds. A large number of compounds are important from the biological point of view [11]. Little attention including azo compounds formed by interaction of sulfonamide drugs as ligands has been reported [12].

Keeping in view of the importance of metal complexes of azo dyes and their wide applications, the present work reports the synthesis, characterization and biological activity studies of two sulfadimidine azo dyes, prepared from 1-hydroxy-2-naphthoic acid or 3-

hydroxy-2-naphthoic acid with sulfadimidine drug, and their Ni(II), Cu(II), Zn(II) and Pd(II) complexes. The thermal decomposition kinetics of all complexes was estimated by Coats-Redfern equation. Also, NiO and CuO nanoparticles were prepared from the thermal decomposition of Ni(II)-L¹ and Cu(II)-L¹ complexes. Finally, the antibacterial activity of the azo dyes and their complexes have been screened against *Escherichia coli* as gram negative and *Staphylococcus aureus* as gram positive bacteria.

2. Experimental

2.1. Materials

All chemicals used were chemically pure grade from BDH. They include Zn(CH₃COO)₂, Cu(CH₃COO)₂.H₂O, NiCl₂.6H₂O, Na₂PdCl₄, 1-hydroxy-2-naphthoic acid, 3-hydroxy-2-naphthoic acid, hydrochloric acid, sodium hydroxide, ammonium hydroxide, sodium chloride, sodium nitrite, (El-Nasr Pharmaceutical Chemicals, Adwic) and sulfadimidine. The organic solvents used included ethanol, acetic acid, dimethylformamide (DMF) and dimethylsulfoxide (DMSO). The organic solvents used in the study were purified by recommended methods [17] or obtained as grade materials from BDH.

2.2. Analysis and Physical Measurements

Carbon, hydrogen and nitrogen were analyzed by standard microanalysis methods using Automatic analyzer CHNS Vario EL III-Elementar, Germany at Microanalytical center, Cairo University, Giza, Egypt. Mass spectra were performed using GC MS-QP 2010 Shimadzu. The ¹H-NMR spectra were recorded using Varian 300 MHz NMR spectrometer at room temperature using TMS (tetramethylsilan) as an internal standard. Infrared spectra were obtained with KBr disc technique using 4100 Jasco-Japan FTIR spectrometer. The electronic absorption spectra in spectroscopic grade dimethylsulfoxide (10⁻⁴ mol L⁻¹ of azo dyes, 5 x 10⁻⁵ mol L⁻¹ of complexes) were measured using Perkin-Elmer lambda 4B UV-Vis spectrophotometer.

The ESR spectra were performed for Cu-L¹ and Cu-L² with an X-band ESR spectrometer (Bruker, EMX) at room temperature using a high sensitivity standard cylindrical resonator (ER 4119 HS) operating at 9.7 GHz with a 100 kHz modulation. Samples with a mass of about 100 mg sample were placed in quartz tube with an internal diameter of 3 mm. The height of the powdered sample inside the tube was ~ 10 mm ensuring a homogenous magnetic field inside the cavity.

Magnetic susceptibilities of the complexes were measured at room temperature using a magnetic susceptibility Cambridge England Sherwood Scientific balance. Molar conductivity of 10⁻³ mol L⁻¹ solutions of the complexes in DMF was measured on the conductivity meter ORION model 150 of 0.6 cell constant.

Thermal analyses were carried out using simultaneous Shimadzu thermogravimetric analyzer TGA-60 H with TA 60 software in dry nitrogen atmosphere at a flow rate of 30 mL min⁻¹ in platinum crucible. The experiment was performed from room temperature up to 600 °C at heating rate 10 °C min⁻¹.

Analysis of the metal ions were carried out by dissolving 20-25 mg of the metal chelate in concentrated nitric acid followed by hydrogen peroxide. The solution was heated gently to fumes and then boiled until the solution becomes clear then the diluted aqueous solutions were neutralized with sodium hydroxide to pH 5.5 and the metal content was determined by the recommended method [18].

X-Ray diffraction was performed using Bruker AXS-D8 Advance X-ray diffractometer with Cu-K α radiation source at 40 kV and 40 mA sec monochromator. The sample is irradiated with a beam of monochromatic x-rays over a variable incident angle range. Interaction with atoms in the sample results in diffracted x-rays when the Bragg equation is satisfied. Resulting spectra are characteristic of chemical composition and phase.

The surface morphological features of NiO and CuO nanoparticles were studied by scanning electron microscope (SEM) using the Quanta FEG-250 SEM instrument.

2.3. Preparation of Azo Dyes

Azo dyes were prepared by dissolving about 2 grams (0.016 mmol) of sulfa drug (sulfadimidine) in 10 mL of concentrated hydrochloric acid. Then a solution of about 0.8 gram of sodium nitrite was added drop wisely in ice bath with continuous stirring to have the diazonium salt. The 1-hydroxy-2-naphthoic acid (coupler of L¹) or 3-hydroxy-2-naphthoic acid (coupler of L²) (1.872 gram 0.016 mmol) was dissolved in 10 mL of sodium hydroxide (2 grams in 100 mL doubly distilled water) and transferred to ice bath. The diazonium salt was added to this solution in ice bath with continuous stirring. The azo dye product was stirred for 15 minutes, then was kept overnight in a refrigerator. The product was acidified with hydrochloric acid (0.1 mol L⁻¹), then filtered and washed with doubly distilled water. These chemical reactions can be represented by Figure 1.

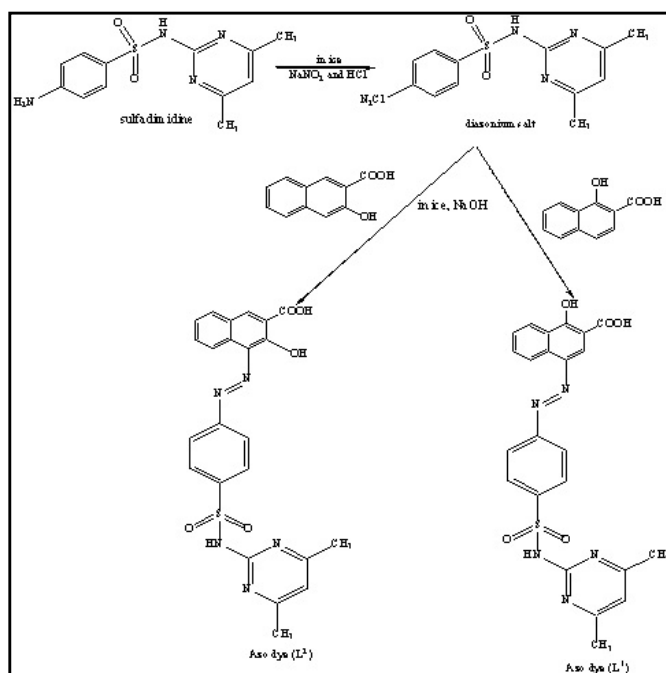


Figure 1: Preparation of azo dyes (L^1 and L^2).

2.4. Preparation of Solid Metal Complexes

The metal complexes were prepared by mixing a hot 20 mL alcoholic solution containing the proper weight of metal ions Cu(II), Ni(II), Zn(II) and Pd(II) with a saturated alcoholic solution containing the requisite amount of azo dyes (L^1 and L^2) to form 1:1 or 1:2 or 2:1 (M:L) chelates. The mixture was allowed to stand on a water bath for 15-30 minutes. Drops of ammonia solution were added slowly with stirring for some of the complexes to enhance complexation. The resulting solid complexes were filtered out, washed with hot ethanol then washed with doubly distilled water. The obtained complexes were desiccated under anhydrous CaCl_2 .

2.5. In Vitro Antibacterial Activity

The antibacterial activity was carried out using a modified Kirby-Bauer disc diffusion method [19] against *Staphylococcus aureus* as Gram-positive and *Escherichia coli* as Gram-negative bacteria. 100 $\mu\text{mol/L}$ of the test bacteria were grown in 10 mL of fresh media until they reached a count of approximately 108 cells/mL. 100 μL of the suspended microbes was spread onto agar plates corresponding to the broth in which they were maintained. Isolated colonies of each organism that might be playing a pathogenic role should be selected from primary agar plates and tested for susceptibility by disc diffusion method [20,21]. Standard disc of Ampicillin was served as a positive control for antibacterial activity. Filter disc impregnated with 10 μL of DMSO (solvent) was used as a negative control. Blank paper discs with a diameter 8.0 mm were impregnated with 10 μL of the tested concentration of the stock solutions. The saturated discs were placed onto surface of the seeded agar plate. Treated plates were inverted and immediately placed into incubator. *Staphylococcus aureus* and *Escherichia coli* were incubated at 35-37 $^\circ\text{C}$ for 24-48 hours. Then the diameter of the inhibition zones was measured in millimeters [19]. The zone diameters were measured with slipping calipers of National Committee for Clinical Laboratory Standards [20,21]. Then the antibacterial activities of each compound could be calculated as a mean of three replicates.

2.6. NiO and CuO Nanoparticles

NiO and CuO nanoparticles are produced from the thermal decomposition of Ni(II)- L^1 and Cu(II)- L^1 complexes in the solid state, respectively, at 600 $^\circ\text{C}$ for 2 hours. The obtained nanoparticles are characterized by XRD, SEM and FTIR methods of analysis.

3. Results and Discussion

3.1. Characterization of Azo Dyes (L^1 and L^2)

The elemental analyses data of the azo dyes (L^1 , L^2) are consistent with the calculated results from empirical formula of each compound. The physical properties and elemental analysis values of such azo dyes are given in Table 1 and 2.

3.2. Mass Spectra of the Free Azo Dyes (L^1 and L^2)

The mass spectra of the azo dyes, Figure 2, were measured in order to confirm their composition.

Since the two azo compounds have the same molecular formula and formula weight ($\text{C}_{23}\text{H}_{19}\text{N}_5\text{SO}_5$, M.Wt. 477.49 g/mol), their mass spectra show a molecular ion peak corresponding to the molecular mass of the respective compounds. Where, mass spectra of L^1 and

L^2 each shows parent peak at $m/z = 477$. This molecular ion peak is in good agreement with the empirical formula as indicated from elemental analyses.

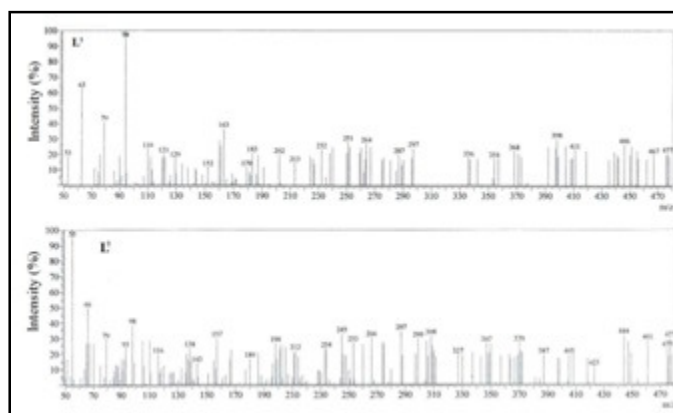


Figure 2: Mass spectra of L^1 and L^2 azo dyes.

3.3. $^1\text{H-NMR}$ Spectra of Azo Dyes

The proton nuclear magnetic resonance spectra of the ligands, L^1 and L^2 , were performed to assign the protons characteristics to different groups in the dyes. The $^1\text{H-NMR}$ spectra of the azo dyes, were obtained in d^6 -dimethylsulfoxide (d^6 -DMSO) solutions using tetramethylsilane (TMS) as internal standard.

The spectra of L^1 and L^2 exhibit signals at δ 3.3-2.2 ppm which assigned to the CH_3 protons attached to pyrimidine ring of sulfa drug [22]. The multiplet signals appeared at δ 7.9-6.5 ppm are assigned to the aromatic protons. The phenolic OH protons appeared as broad signal in the range 12.075-12.12 ppm is due to intermolecular hydrogen bonds [23]. The spectra of the two ligands exhibit broad signals at δ 13.8, 13.7 ppm due to intramolecular hydrogen bond. This band can be assigned to carboxylic OH proton for L^1 and L^2 , respectively.

3.4. Characterization of the Chelates

Elemental analyses and some physical properties of the isolated complexes are listed in Table 1 and 2. It is worthy to mention that the found values of different elements were in good agreement with the calculated one according to the proposed molecular formulae. The formed complexes have different stoichiometric ratios. Ni(II) forms with L^1 and L^2 ligands, (2:2) (M:L), $[\text{Ni}_2\text{L}^2\cdot 4\text{H}_2\text{O}]$ and 1:1 (M:L) $[\text{Ni}\cdot\text{L}\cdot\text{Cl}\cdot 3\text{H}_2\text{O}]$ complexes, respectively. Cu(II) forms binuclear complexes $[\text{Cu}_2\cdot\text{L}^1\cdot\text{OH}\cdot 3\text{H}_2\text{O}]\cdot 4\text{H}_2\text{O}$ and $[\text{Cu}_2\cdot\text{L}^2\cdot\text{OH}\cdot 3\text{H}_2\text{O}]$. On other hand, Zn(II) forms complexes with stoichiometric ratio (1:2) (M:L) with the two azo dyes $[\text{Zn}\cdot 2\text{L}\cdot\text{H}_2\text{O}\cdot \text{C}_2\text{H}_5\text{OH}]\cdot \text{H}_2\text{O}$. Pd(II) forms mononuclear complexes (1:1) (M:L), $[\text{Pd}\cdot\text{L}\cdot\text{Cl}\cdot\text{H}_2\text{O}]$ where L is L^1 or L^2 azo dyes. The isolated complexes are insoluble in most organic solvent and moderately soluble in DMSO and DMF.

The molar conductivity of 10^{-3} mol L^{-1} solutions in DMSO is in the range of 0-50 $\text{ohm}^{-1} \text{cm}^2 \text{mol}^{-1}$ is the range of non electrolytes [24,25]. In the present study, the molar conductance values of metal complexes in DMSO are in the range (6.2-49) $\text{ohm}^{-1} \text{cm}^2 \text{mol}^{-1}$ may be taken as evidence for the non-electrolytic nature of these complexes.

Symbol	Compound	Formula	MWt (g/mol)	Molar conductance ($\text{ohm}^{-1} \text{cm}^2 \text{mol}^{-1}$)	Elemental analyses				
					%C Calcd. (Found)	%H Calcd. (Found)	%N Calcd. (Found)	%S Calcd. (Found)	%M Calcd. (Found)
L^1	L^1	$\text{C}_{23}\text{H}_{19}\text{N}_5\text{SO}_5$	477.49	-	57.85 (57.93)	4.01 (4.04)	14.67 (14.05)	6.72 (6.14)	-
Ni(II)- L^1	$[\text{Ni}\cdot\text{L}^1\cdot\text{Cl}\cdot 3\text{H}_2\text{O}]$	$\text{C}_{23}\text{H}_{24}\text{NiClN}_5\text{O}_8\text{S}$	625.69	25.9	44.15 (44.60)	3.87 (3.78)	11.19 (10.66)	5.12 (5.19)	9.38 (9.78)
Cu(II)- L^1	$[\text{Cu}_2\cdot\text{L}^1\cdot\text{OH}\cdot 3\text{H}_2\text{O}]\cdot 4\text{H}_2\text{O}$	$\text{C}_{23}\text{H}_{31}\text{CuN}_5\text{O}_{13}\text{S}$	744.41	18.4	37.12 (37.16)	4.19 (4.20)	9.41 (9.91)	4.31 (4.01)	17.07 (17.00)
Zn(II)- L^1	$[\text{Zn}\cdot 2\text{L}^1\cdot\text{H}_2\text{O}\cdot \text{C}_2\text{H}_5\text{OH}]\cdot \text{H}_2\text{O}$	$\text{C}_{48}\text{H}_{46}\text{ZnN}_{10}\text{O}_{13}\text{S}$	1099.46	11.7	52.44 (52.28)	4.22 (4.36)	12.72 (12.53)	5.83 (5.72)	5.95 (6.02)
Pd(II)- L^1	$[\text{Pd}\cdot\text{L}^1\cdot\text{Cl}\cdot \text{H}_2\text{O}]$	$\text{C}_{23}\text{H}_{20}\text{PdClN}_5\text{O}_6\text{S}$	636.35	6.1	43.41 (44.19)	3.17 (3.24)	11.00 (10.89)	5.04 (4.98)	16.72 (16.43)

Table 1: Analytical and physical data of the ligand (L^1) and its metal complexes.

Symbol	Compound	Formula	MWt (g/mol)	Molar conductance (ohm ⁻¹ cm ² mole ⁻¹)	Elemental analyses				
					%C Calcd. (Found)	%H Calcd. (Found)	%N Calcd. (Found)	%S Calcd. (Found)	%M Calcd. (Found)
L ²	L ²	C ₂₃ H ₁₉ N ₅ SO ₅	477.49	-	57.85 (58.00)	4.01 (4.08)	14.67 (14.51)	6.72 (6.21)	-
Ni(II)-L ²	[2Ni.2L ₂ .4H ₂ O]	C ₄₆ H ₄₂ NiN ₅ O ₁₄ S ₂	1136.38	6.2	48.62 (48.45)	3.01 (3.13)	12.32 (12.30)	5.64 (5.40)	10.33 (10.24)
Cu(II)-L ²	[Cu ₂ .L ² .OH ⁻ .3H ₂ O]	C ₂₃ H ₂₃ CuN ₅ O ₉ S	672.43	12.2	41.08 (41.07)	3.45 (3.49)	10.41 (10.24)	4.77 (4.98)	18.90 (18.87)
Zn(II)-L ²	[Zn.2L ² .H ₂ O.C ₂ H ₅ OH]H ₂ O	C ₄₈ H ₄₆ ZnN ₅ O ₁₃ S	1099.46	40.0	52.44 (52.30)	4.22 (4.01)	12.72 (13.20)	5.83 (6.07)	5.95 (6.00)
Pd(II)-L ²	[Pd.L ² .Cl ⁻ .H ₂ O]	C ₂₃ H ₂₀ PdClN ₅ O ₆ S	636.35	15.9	43.41 (44.07)	3.17 (3.15)	11.00 (10.79)	5.04 (4.98)	16.72 (16.33)

Table 2: Analytical and physical data of the ligand (L²) and its metal complexes.

3.5. Electronic Spectra and Magnetic Moment Measurements

The electronic absorption spectra of azo dyes and their complexes were performed in dimethyl sulfoxide (DMSO). The position of the band maxima and the magnetic moment values of the complexes are mentioned in Table 3.

Symbol	ν kK	B.M.
L ¹	27.62, 20.28	-
Ni(II)-L ¹	17.36, 23.25, 20.83	2.9
Cu(II)-L ¹	17.54, 20.49	2.84
Zn(II)-L ¹	20.96, 28.17	0.0
Pd(II)-L ¹	19.76, 26.67	0.0
L ²	23.64, 20.08	-
Ni(II)-L ²	16.53, 23.25, 23.75	6.2
Cu(II)-L ²	17.64, 19.763	2.8
Zn(II)-L ²	23.47, 27.70	0.0
Pd(II)-L ²	19.34, 24.15	0.0

Table 3: Electronic absorption bands and magnetic moments of azo dyes and their complexes.

The electronic absorption spectra of L¹ and L² azo dyes exhibit bands at 362 and 423 nm (27.62 and 23.64 kK), respectively, assigned to the π - π^* transitions born out from the conjugation of benzene rings. Another band observed in the electronic absorption spectra of L¹ and L² at 493 and 498 nm (20.28 and 20.08 kK), respectively. This band due to π - π^* transitions within the azo group (N=N) influenced by an intramolecular charge-transfer (CT transition) involving the whole molecule. The charge-transfer (CT) band would originate from the OH group (donor) in the naphthol ring linked to the -N=N- bridge, which behaves as an acceptor. In the electronic spectra of all complexes, this band shows hypsochromic shift, Table 3.

The electronic spectra of Ni(II)-L¹ and Ni(II)-L² complexes show absorptions typical of an octahedral geometry at 17.36 and 16.53 kK, respectively, assigned to $^3A_{2g} \rightarrow ^3T_{1g}(F)$ (ν_2), while the band at 23.25 kK in the spectra of the two complexes is due to $^3A_{2g} \rightarrow ^3T_{1g}(P)$ (ν_3) transition [26]. Ni(II)-L¹ shows magnetic moment of 2.9 BM. This value indicates paramagnetic nature and an octahedral geometry has been assigned [27] to this complex. On other hand, the Ni(II)-L² complex shows unusual magnetic moment value (6.2 BM) which could be considered as 2:2 (M:L) complexes where two ligand molecules are coordinated to two metal ions. This value (3.1 B.M. per metal ion) is within the range (2.9-3.3 BM), found for paramagnetic complex of Ni(II) with octahedral geometry [28].

While, the electronic spectra of binuclear Cu(II)-L¹ and Cu(II)-L² complexes exhibit bands at 17.54 and 17.64 kK, respectively, which can be assigned to $^2B_{1g} \rightarrow ^2A_{1g}$ transition [29,30]. This transition, as well as, the value of the magnetic moment measurement of the two complexes ($\mu_{\text{eff}} = 1.42$ and 1.40 BM per metal ion) suggest a square-planar stereochemistry [31] of these complexes. The low value of μ_{eff} for the two complexes can be explained on the bases of anti-ferromagnetic interactions [32].

The Zn(II) complexes were expectedly diamagnetic. Zn(II) complexes show only the charge transfer transitions, no d-d transition are expected. In the electronic spectra of Zn(II)-L¹ and Zn(II)-L² complexes, an absorption band at 20.96 and 23.47 kK, respectively, was observed which is compatible with octahedral structure [33,34].

Also, the palladium complexes are diamagnetic as expected for square planar d⁸ systems. The electronic spectra of the complexes under study display band at 19.76 kK for Pd(II)-L¹ and at 19.34 kK for Pd(II)-L². These bands may be assigned to $^1A_{1g} \rightarrow ^1B_{1g}$ (ν_2) transition. The electronic spectra of these complexes indicate the square planar geometry around the Pd(II) ion [35,36].

The electronic spectra of all complexes exhibit band in the range 19.76-28.17 kK, Table 3, can be attributed to ligand to metal charge transfer [37].

3.6. ESR spectra of Cu(II) Complexes

The ESR spectral studies of Cu (II) complexes, Figure 3, provide information of the metal ion environment. The magnetic parameters measured in this study are related to the structure of the paramagnetic species, the number of ligands and the bonding parameters and spatial arrangements of the ligands around the central metals ion. The room temperature X-band ESR spectra of polycrystalline Cu (II) complexes for the two ligands were recorded. The ESR spectra of these complexes are quite similar and exhibit an axially symmetric g-tensor parameters with $g_{\parallel} \perp 2.0023$ indicating that the unpaired electron most likely reside in dx^2-y^2 ground state [38] characteristic of square planar, square pyramidal or octahedral geometry [39]. Table (4) summarizes the g_{\parallel} , g_{\perp} and G values. Kivelson and Neiman [40] have demonstrated that for covalent environments g_{\parallel} is less than 2.3 and for ionic environment this is usually ≥ 2.3 . The calculated g_{\parallel} for the two complexes is less than 2.3, Table (4), indicating the presence of considerable covalency. The evaluation of ESR covalency parameters also supports this. Also the g values are related by the expression $G = (g_{\parallel}-2)/(g_{\perp}-2)$. If the value of $G > 4$, the exchange interaction is negligible whereas if $G < 4$, a considerable exchange interaction is indicated in the solid complexes. Since G values are lower than 4 for the studied azo complexes, Table 4, indicating the presence of copper-copper exchange reaction for these binuclear complexes [41]. A forbidden magnetic dipole transition for the two complexes is observed at half-field (c. 1500 G, $g = 4.0$) but the intensity is very weak. The appearance of a half-field signal confirms the magnetic interaction between the two Cu(II) ions in 2:1 M:L complexes. The low magnetic moment values for the binuclear Cu-azo complexes indicate the presence of strong exchange coupling between Cu (II) center in the solid state [42].

Compound	g_{\parallel}	g_{\perp}	gav.	$A_{\parallel} \times 10^{-4} \text{ cm}^{-1}$	G	$g_{\parallel}/A_{\parallel}$
Cu(II)-L ¹	2.21	2.06	2.11	173	3.50	128
Cu(II)-L ²	2.24	2.07	2.13	177	3.42	127

Table 4: ESR data of Cu(II)-L¹ and Cu(II)-L² complexes.

In order to quantify the degree of distortion of the copper (II) complexes, f factor is selected is given by $g_{\parallel}/A_{\parallel}$ from the ESR spectra. Its value ranges between 105 and 135 cm^{-1} for square planar complexes, depending on the nature of coordinated atoms. In the presence of tetrahedrally distorted structure, the value rise up to 250 cm^{-1} as shown in Table 4. The $g_{\parallel}/A_{\parallel}$, 128, 127 cm^{-1} , values of Cu(II)-L¹ and Cu(II)-L² complexes lie within the range expected for square planar arrangement [43].

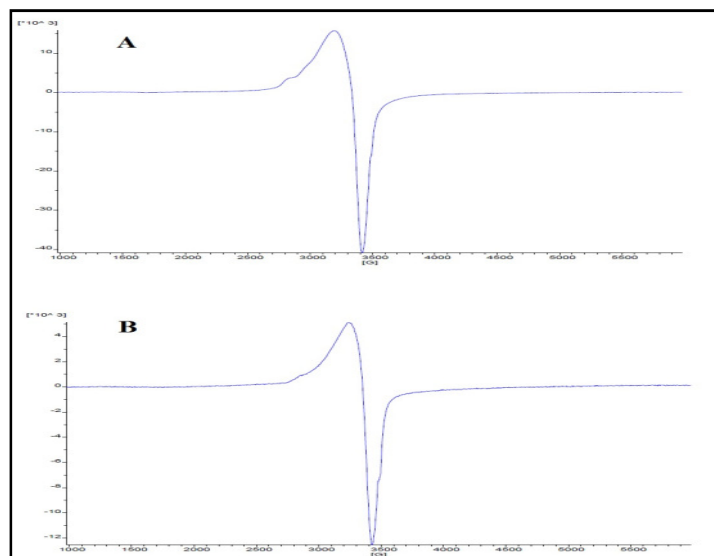


Figure 3: The ESR spectra of Cu(II)-L¹ (A) and Cu(II)-L² (B) complexes.

3.7. ¹H-NMR of the Zn(II) complexes

In the ¹H-NMR spectra of Zn(II)-L¹ and Zn(II)-L² complexes, the absence of the signals assignable to phenolic OH protons of naphthoic acid moiety, confirming its participation in the chelate formation. On other hand, the signals due to the carboxylic group protons shifted downfield and appear as doublet at δ 8.8 ppm for the two complexes due to the perturbing effect of the coordinated metal ion to two molecules of ligand. The multiplet signals of the aromatic protons are shifted to higher field and appeared at δ 7.2-8.3 pm. The signal appeared at δ 3.4 and 3.9 ppm in the ¹H-NMR spectra of Zn-L¹ and Zn-L², respectively, can be attributed to the water molecules in these complexes. Thus, the spectra confirm the involvement of the hydroxyl group after deprotonation in a monodentate mode in metal coordination and formation of (1:2) (M:L) complexes.

3.8. FTIR spectra of the complexes in a comparison with the IR spectrum of the free ligands

The existence of numerous coordination sites in the ligand offer variable bonding modes; however information on the coordinating sites of ligands to metal ions could be provided by comparison of the IR spectra of the ligands L^1 and L^2 and their metal ions complexes.

The most characteristics infrared bands of the free ligands and those of their metal complexes are given in Table (5). It can be noticed that;

1. The spectra of the ligands showed a broad band at 3417 cm^{-1} due to the OH stretching band of phenolic OH group. The broadening of this band indicates that the OH⁻ is involved in hydrogen bonding. This band in the complexes was replaced by new peaks within the range $3425\text{-}3417\text{ cm}^{-1}$ due to coordinated or lattice water or OH⁻ ions attached to the metal ions to satisfy their coordination numbers.
2. The band at 3236 cm^{-1} assigned to ν (NH) in the free ligand remained more or less at the same position in the complexes. The stretching vibration for C=O of the -COOH group, observed at $\sim 1640\text{ cm}^{-1}$, for L^1 and L^2 disappeared in the Cu(II) (2:1) M:L and Zn(II) (1:2) M:L complexes indicating the participation of this group in complex formation, table (5). The IR of Ni(II) and pd(II) complexes showed the C=O stretching at the same position as the ligand suggesting that this group was not involved in coordination.
3. The stretching vibration for C=N group of the pyrimidine ring in the free ligands was found at $\sim 1554\text{ cm}^{-1}$, Table 5. This band appeared almost at the same position in the spectra of Zn(II) complexes, which can be taken as an evidence that C=N group is not taking part in the coordination to the metal center. For Cu(II), Ni(II) and pd(II) complexes this band is splitted into two bands, Table 5. The first band appeared almost at the same position while the second band is shifted to lower or higher wave numbers indicating that one nitrogen of the pyrimidine ring was involved in the coordination to the metal ion while the other one remained free. Indicating the presence of different chemical environments.
4. The bands due to ν (N=N) group which appeared in the spectra of L^1 and L^2 at 1435 and 1431 cm^{-1} , respectively. This band don't show significant shift in the spectra of the metal complexes, Table 5, indicating that N=N group do not participate in complex formation. In case of Ni(II)- L^2 complex, this band was shifted to higher wave number by 52 cm^{-1} upon chelation which can be taken as an evidence for the coordination of N=N to the metal center.
5. In the IR spectra of ligands ν (S=O) asymmetric and symmetric vibrations appeared at 1342 cm^{-1} and 1144 cm^{-1} for L^1 and at 1354 and 1142 cm^{-1} for L^2 , respectively. These bands were shifted to lower frequency in Cu(II), Ni(II) and pd(II) complexes indicating the coordination of sulfonamide oxygen to the metal center in the enolic form through deprotonation [44]. In Zn(II) complexes, this band cannot be identified because in this complex the stiochiometric ratio is (1:2) (M:L) and the fine splitting of the bands is not clear.
6. The two bands appearing in the spectra of L^1 and L^2 at 1190 and 1222 cm^{-1} correspond to the two ν C-OH stretching vibrations of the C-OH in carboxylic and phenolic groups, respectively. The first band (at 1190 cm^{-1}) was found to appear at almost the same position in the spectra of the metal complexes which indicate that the C-OH of COOH group is not involved in complex formation. The second band (at 1222 cm^{-1}) was shifted to higher frequency and was observed at 1265 , 1253 and 1261 cm^{-1} for Zn(II), Cu(II) and Ni(II), respectively indicating that the metal ions are coordinated through the oxygen atom of the phenolic group after deprotonation.

Symbol	ν_{OH}	ν_{NH}	$\nu_{\text{C=O}}$	$\nu_{\text{C=N}}$	$\nu_{\text{N=N}}$	$\nu_{\text{(S=O)asy.}}$ $\nu_{\text{(S=O)sym}}$	$\nu_{\text{M-O}}$	$\nu_{\text{M-N}}$
L^1	3417	3236	1640	1553	1435	1342 1144	-	-
Cu(II)- L^1	3425	3236	-	1553,1516	1427	1268 1080	582	424
Ni(II)- L^1	3425	3236	1640	1553,1508	1435	1250 1080	510	459
Zn(II)- L^1	3417	3244	-	1553	1438	- 1141	510	-
Pd(II)- L^1	3417	3236	1640	1553	1435	1275 1080	530	455
L^2	3479	3236	1639	1554,1536	1431	1354 1142	-	-
Cu(II)- L^2	3417	3240	-	1555,1546	1438	1284 1080	555	439
Ni(II)- L^2	3417	3240	1640	1554,1548	1483	1261 1080	551	435
Zn(II)- L^2	3417	3244	-	1554	1443	- 1141	535	-
Pd(II)- L^2	3417	3236	1640	1540,1516	1427	1311 1145	586	466

Table 5: IR spectral bands of the ligands and their metal chelates.

- A new band in the IR spectra of all the metal chelates in the region 586-510 cm^{-1} which was attributed to $\nu\text{M-O}$. In the IR spectra of Ni(II), Cu(II) and Pd(II) complexes, a new band appears at 466-424 cm^{-1} may be due to the stretching vibration of $\nu\text{M-N}$.
- The IR spectra of the free ligands L^1 and L^2 exhibit a broad absorption band at $\sim 4416 \text{ cm}^{-1}$ which is assigned to the intra and inter-molecular hydrogen bond vibrations which is not observed in the spectra of the complexes indicating the involvement of the deprotonated hydroxyl oxygen in complexation.

3.9. Thermal Studies

The results of the thermal analysis of the L^1 complexes are given in Table 6. All complexes of L^1 were thermally decomposed till 600 $^\circ\text{C}$ at heating rate 10 $^\circ\text{C min}^{-1}$.

The first decomposition step in the TG curve of Ni(II)- L^1 complex from the ambient till 158 $^\circ\text{C}$ is due to the elimination of three water molecules of coordination (8.66%, calcd. 8.64%). The second step started at 158 $^\circ\text{C}$ and ended at 263 $^\circ\text{C}$ with mass loss of 5.56%, calcd. 5.67%, can be attributed to the elimination of one chloride ion which participate in the coordination sphere of the divalent positive metal ion for its charge balance achievement. Then the organic part of the chelate decomposes and shows weight loss of 36.68 % (calcd. 36.76%) at 263-430 $^\circ\text{C}$ and another weight loss of 36.99% (calcd. 37.08%) at 430-588 $^\circ\text{C}$. The stable NiO at 588 $^\circ\text{C}$ is formed as final product Table 6.

For Cu(II)- L^1 complex, the loss in weight of 9.64%, calcd. 9.68, at 19-70 $^\circ\text{C}$ may be due to the loss of four lattice water molecules. On other hand, the loss at 7.20%, calcd 7.26% within the temperature range from 70 to 215 $^\circ\text{C}$ can be attributed to the loss of three water molecules from the coordination sphere of the metal ion. A continuous loss in weight occurs and the organic part of the complex decompose in two steps, the first step occurs at 215-350 $^\circ\text{C}$ with weight loss of 37.49% (calcd. 37.34%) and the second one occurs at 350-461 $^\circ\text{C}$ with weight loss of 23.57% (calcd. 23.51%) till the formation of CuO as a final product (21.31%, calcd. 21.37%).

The TG Curve of Zn(II)- L^1 complex shows loss in weight corresponding to loss of one water molecule of crystallization with mass loss 1.67% (calcd. 1.64%) in the temperature range from 38 to 96 $^\circ\text{C}$. Another mass loss of 1.67% (calcd. 1.64%) occurs in the temperature range of 96-215 $^\circ\text{C}$ due to one water molecule of coordination. The step within temperature range 215-273 $^\circ\text{C}$ with mass loss 4.17% (calcd. 4.19%) is due to elimination of one ethanol molecule from the coordination sphere of the chelate. Then there is a continuous decomposition of the complex occurs with weight loss of 26.48% (calcd. 26.47%) in the temperature range of 273-450 $^\circ\text{C}$ and weight loss of 57.10% (calcd. 57.12%) at 450-600 $^\circ\text{C}$ till the final product is formed at 600 $^\circ\text{C}$ as metal oxide i.e. ZnO (7.50%, calcd. 7.40%).

In the TG curve of Pd(II)- L^1 complex, the mass loss of 2.97%, calcd. 2.83%, occurs in the temperature range of 80-136 $^\circ\text{C}$ is due to the removal of one water molecule of coordination. The loss observed at 136-180 $^\circ\text{C}$ due to elimination of one chloride ion (5.36%, calcd. 5.57%). Then this curve shows two steps of weight losses at 180-473 $^\circ\text{C}$ range that is attributed to thermal decomposition of the complex. Where, the first weight loss occurs at 180-344 $^\circ\text{C}$ (27.40, calcd. 27.50%). The second step with weight loss of 46.27% (calcd. 45.73%) at 344-473 $^\circ\text{C}$. At 473 $^\circ\text{C}$ there is a residue, PdO, corresponding to 18.90 % (calcd. 19.23 %) formed.

3.10 Kinetic Studies

The thermodynamic parameters of the two thermal degradation steps (decomposition of the organic part of the complex) were calculated using Coats-Redfern equation [45].

For first order process ($n = 1$), Coats-Redfern equation is used in the following form:

$$\log \left[\frac{-\log(1-X)}{T^2} \right] = \log \left[\frac{AR}{\beta E_a} \left[1 - \frac{2RT}{E_a} \right] \right] - \frac{E_a}{2.303RT}$$

Where: x is the fraction decomposed, T is the absolute temperature, R is the gas constant and β is the heating rate, 10 $^\circ\text{C/min}$. The term $1-2RT/E_a \approx 1$ so, the plot of $\log \left[\frac{-\log(1-X)}{T^2} \right]$ against $1000/T$ would give a straight line where E_a and A (Arrhenius constant) were calculated from the slope and the intercept, respectively. The data are summarized in Table 7.

Complex	Temp. range $^\circ\text{C}$	Weight loss % Calcd. (Found)	Removed species	Metal residue % Calcd. (Found)	Temp., $^\circ\text{C}$
[Ni.L ¹ .Cl.3H ₂ O]	-	-	-	11.93 (11.78)	588
	33-158	8.64 (8.66)	3 H ₂ O		
	158-263	5.67 (5.56)	Cl ⁻		
	263-430	36.76 (36.67)	C ₁₂ H ₁₀ N ₂ O ₃		
[Cu ₂ .L ¹ .OH.3H ₂ O].4H ₂ O	430-588	37.08 (36.99)	C ₁₀ H ₆ N ₃ SO ₂		
	19-70	9.68 (9.64)	4 H ₂ O	21.37 (21.31)	462
	70-215	7.26 (7.20)	3 H ₂ O		
	215-350	37.34 (37.49)	C ₁₃ H ₁₆ N ₃ SO ₂		
[Zn.2L ¹ .H ₂ O. C ₂ H ₅ OH].H ₂ O	350-461	23.51 (23.57)	C ₉ H ₇ N ₂ O ₂		
	38-96	1.64 (1.67)	1H ₂ O	7.40 (7.50)	600
	96-215	1.64 (1.67)	1H ₂ O		
	215-273	4.19 (4.17)	C ₂ H ₅ OH		

[Pd.L ¹ .Cl ⁻ .H ₂ O]	273-450	26.47 (26.48)	C ₁₃ H ₁₁ N ₂ SO ₄		
	450-600	57.12 (57.10)	C ₃₂ H ₂₀ N ₈ SO ₅		
	-	-		19.23 (18.90)	473
	80-136	2.83 (2.97)	1H ₂ O		
	136-180	5.57 (5.36)	Cl ⁻		
	180-343	27.50 (27.40)	C ₉ H ₇ N ₂ O ₂		
	343-473	44.73 (46.27)	C ₁₃ H ₁₃ N ₃ SO ₃		

Table 6: Thermogravimetric analysis data of complexes of azo dye L¹

Complex	E (kJ mol ⁻¹)	A (s ⁻¹)	ΔH* (kJ mol ⁻¹)	ΔS* (kJ mol ⁻¹ K ⁻¹)	ΔG* (kJ mol ⁻¹)	r ²
Ni(II)-L ¹	24.56	1.39x10 ¹²	18.85	-0.40	295.22	0.98
	20.71	2.07x10 ¹²	14.20	-0.40	327.46	0.97
Cu(II)-L ¹	19.32	1.48x10 ¹²	14.45	-0.40	249.12	0.97
	11.48	1.90x10 ¹²	5.57	-0.40	289.98	0.98
Zn(II)-L ¹	21.47	2.49x10 ¹²	16.12	-0.39	271.35	0.99
	53.19	3.35x10 ¹²	46.71	-0.43	385.49	0.99
Pd(II)-L ¹	14.25	2.85x10 ¹²	9.41	-0.39	239.56	0.99
	42.57	3.43x10 ¹⁰	37.15	-0.43	319.49	0.98

Table 7: Kinetic Parameters of the complexes using Coats-Redfern equation.

Zn(II)-L¹ complex shows the highest activation energy averaged to 37.33 kJ mol⁻¹ indicating its considerable thermal stability this may be due to that Zn(II) forms (1:2) (M:L) complex. While, Cu(II)-L¹ complex has moderate thermal stability as indicated from the value of its activation energy, Table 7. The relative thermal stability as reflected from the average value of the activation energies of the chelates is in the order Zn(II)-L¹ > Pd(II)-L¹ > Ni(II)-L¹ > Cu(II)-L¹.

The entropy of activation (ΔS*), enthalpy of activation (ΔH*), and the free energy change of activation (ΔG*) were calculated using the following equations:

$$\Delta S^* = 2.303 \left[\log \frac{Ah}{KT} \right] R$$

$$\Delta H^* = E - RT$$

$$\Delta G^* = \Delta H - T \Delta S^*$$

Where, K is the Boltzmann constant, h the plank's constant and T is the DTG peak temperature.

The calculated values of ΔS*, ΔH* and ΔG* and linear correlation coefficients r², for the decomposition steps are given in Table 7.

The average of ΔS* values of the decomposition stages for the complexes were found to be negative. The negative entropies of activation of complexes indicated that the studied complexes are in more ordered state. The positive sign of ΔG* suggests that the thermal decomposition steps are non-spontaneous process.

3.11. NiO and CuO nanoparticles

The azo dye L¹ complexes with Ni(II) and Cu(II) ions are thermally decomposed in solid state at 600 °C for 2 hours. The structure of the produced NiO and CuO nanoparticles was studied using XRD, SEM and FTIR analysis.

The phase composition purity and structure of samples were examined using XRD. Figure 4, shows XRD pattern of NiO nanoparticles. From the figure it can be seen that the diffraction peaks are broad due to the small size effect. The peaks positions appearing at 2θ = 37.16°, 43.25°, 62.85° and 75.35°. These diffraction peaks can be perfectly indexed to the face centered cubic (FCC) crystalline structure of NiO, not only in peak position, but also in their relative intensity which is in accordance with that of the standard spectrum (JCPDS, No. 04-0835). The XRD, pattern shows that the sample is single phase and no diffraction peaks characteristic of any other impurities were detected. The crystallite size, Table 8, was found to vary between 29.3-38.4 nm. From the above results it can be concluded that the NiO nanoparticles obtained from the decomposition of Ni(II)-L¹ complex have high purity.

The surface morphological features of NiO nanoparticles were studied by scanning electron microscope (SEM). The SEM micrograph of the prepared NiO crystals is shown in Figure 5. The SEM micrograph shows cubic crystallites. Moreover, the micrograph also shows the agglomeration of the crystallites. The agglomeration may occur due to the crystallites being of nanodimension. The observation of some larger nanoparticles may be attributed to the fact that NiO nanoparticles have the tendency to agglomeration due to their high surface energy and high surface area tension of the ultrafine nanoparticles.

Figure 4 shows XRD pattern of CuO nanoparticles. All peaks can be indexed to the monoclinic crystals system CuO [46]. No characteristics peaks of any impurities were detected, suggesting the high quality of CuO nanoparticles obtained from the thermal decomposition of Cu(II)-L¹ complex. The presence of sharp structural peaks in XRD pattern and crystallite size less than 100 nm suggested the nano crystalline nature of CuO nanoparticles. Figure 5 shows the typical SEM image of CuO nanoparticles. The SEM micrograph shows the agglomeration of the crystallite and the crystallite size is the same as that obtained from XRD analysis.

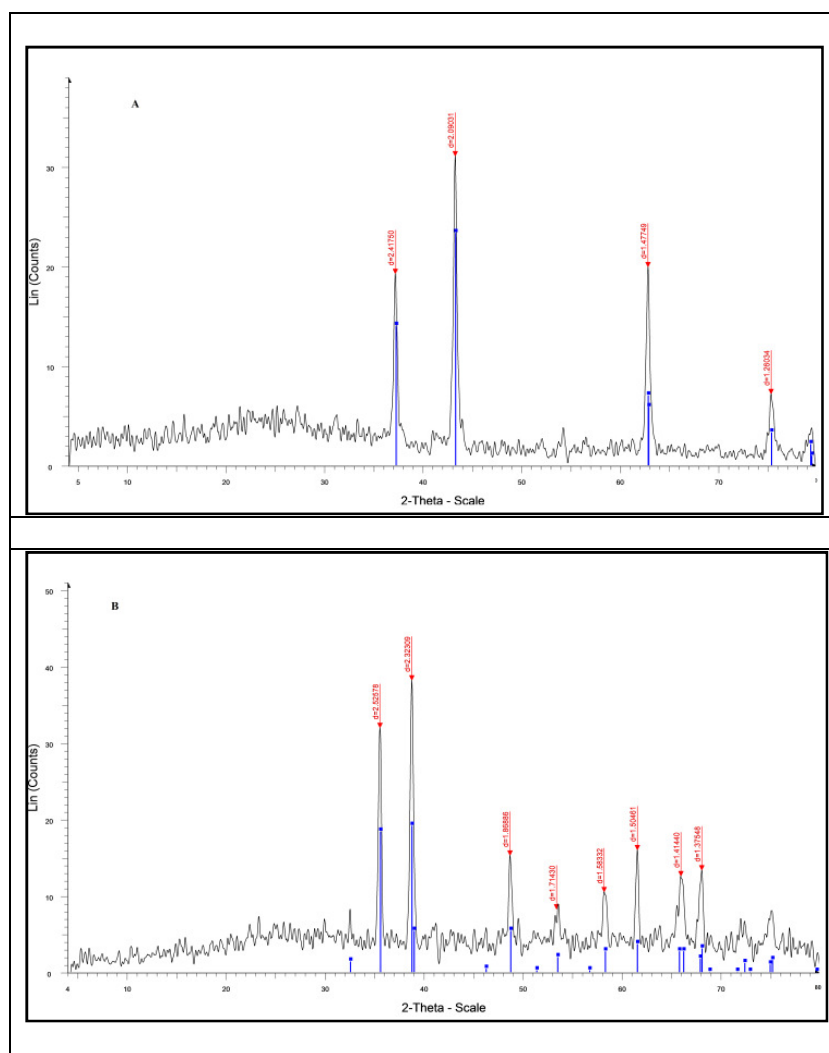


Figure 4: XRD of NiO (A) and CuO (B) nanoparticles.

The FTIR spectra of NiO and CuO nanoparticles has several significant absorption peaks recorded in rang of $4000-400\text{ cm}^{-1}$. The broad absorption band centered at 3421 and 3437 cm^{-1} for NiO and CuO nanoparticles, respectively, is assigned to O-H stretching vibration may be caused by the absorbed water molecules. Since the nano crystalline materials exhibit a high surface to volume ration and thus absorb moisture. The band at 1624 cm^{-1} is attributed to H-O-H bending vibration mode. While the band at 1113 cm^{-1} may be due to the O-H bond deformation assigned to the water adsorption. The broad absorption band in the region $432-448\text{ cm}^{-1}$ is assigned to Ni-O stretching vibration mode [47]. The broadness of the band indicated the nano crystalline nature of the sample. The FTIR spectrum of CuO nanoparticles shows band at 525 cm^{-1} which can be assigned to the vibration of Cu(II)-O bond. The metal oxygen frequencies observed for the respective metal oxides are in close agreement with literature vales [48,49].

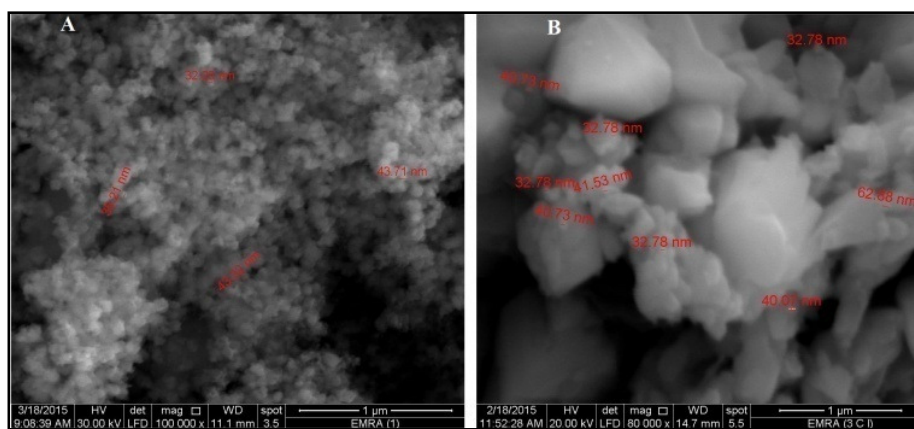


Figure 5: The SEM micrograph of the prepared NiO (A) and CuO (B) nanoparticles crystals.

3.12. Antibacterial Activity Study

The prepared azo dye ligands (L^1 and L^2) and their complexes are evaluated for *in vitro*-antibacterial activity against *Staphylococcus aureus* as Gram-positive and *Escherichia coli* as Gram-negative bacteria using Ampicillin as standard, Figure 6. L^1 azo dye shows good antibacterial activity. Cu(II)- L^1 and Ni(II)- L^1 complexes possesses appreciable antibacterial activity against *Staphylococcus aureus* only. Zn(II)- L^1 complex displays activity against both bacteria but that against *Staphylococcus aureus* is higher than the free azo dye, L^1 , on other hand, Pd(II)- L^1 complex has no effect on these bacteria. L^2 azo dye and its complexes has no effect on the bacteria except Zn(II)- L^2 and Cu(II)- L^2 complexes. It is found that Zn(II)- L^2 complex has significant antibacterial activity against *Staphylococcus aureus* and *Escherichia coli*. Cu(II)- L^2 complex shows antibacterial activity against *Staphylococcus aureus* only. So, it is noticed that L^1 , Zn(II)- L^1 and Zn(II)- L^2 compounds were active as antibacterial agent against *Staphylococcus aureus* and *Escherichia coli*.

Nanoparticle	Angle (2θ)	d-value (Å)	Intensity %	Crystalline size (nm)
NiO	37.1	2.42	61.9	29.3
	43.25	2.09	100.0	34.6
	62.85	1.48	64.1	38.4
	75.35	1.26	23.1	32.1
CuO	35.51	2.53	83.7	40
	38.73	2.32	100.0	38.3
	48.68	1.87	40.0	30.8
	53.40	1.71	21.6	14.4
	58.22	1.58	27.5	30.2
	61.59	1.51	41.8	63.7
	65.99	1.41	32.9	23.5
	68.11	1.38	34.9	53

Table 8: XRD data of NiO and CuO nanoparticles.

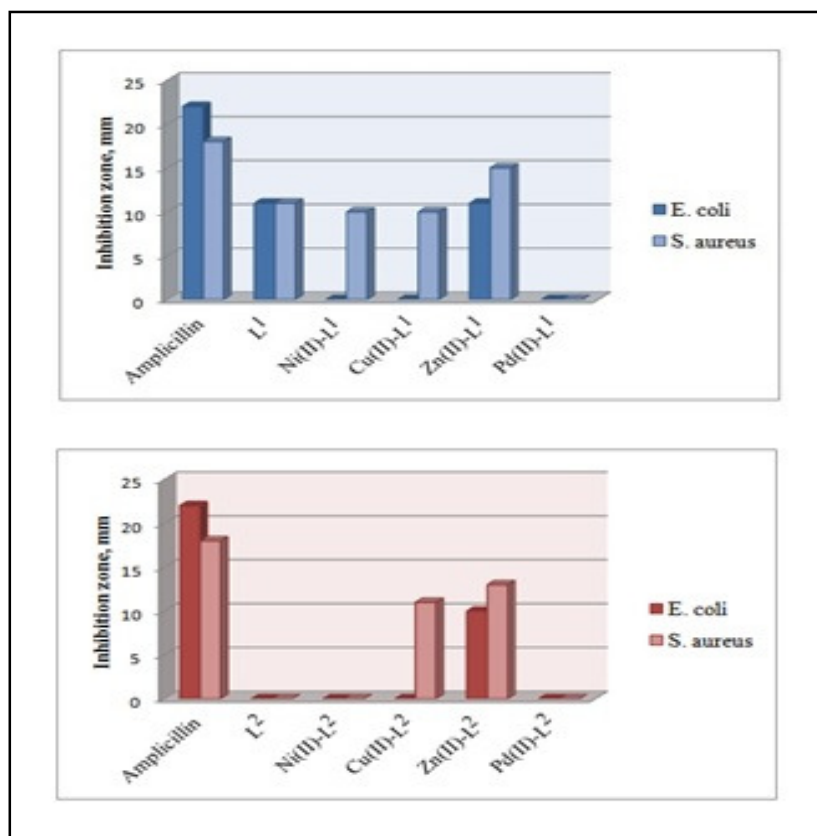


Figure 6: Antibacterial activity of L^1 , L^2 and their complexes.

4. Conclusions

Concerning the ligating properties of the azo dyes and the geometry of their metal complexes, it can be concluded that:

The two ligands L^1 and L^2 have mainly the same ligating properties in all complexes except with Ni(II) as L^1 acts as mono basic bidentate ligands and the chelation occurs through the sulfonamide group [-SO₂-NH-] in the enolic form and nitrogen of pyrimidine ring to form 1:1 (M:L) Ni(II)- L^1 complex, Figure 7A. On the other hand L^2 forms with Ni(II) 2:2 (M:L) complex confirmed by its unusual magnetic moment value (6.2 BM), Figure 7B. Both complexes have octahedral structure. Cu(II) forms binuclear complexes, Figure 8. On the other hand, Zn(II) forms complexes with stoichiometric ratio (1:2) (M:L), Figure 9, Each ligand acts as a mono basic bidentate and the chelation occurs through deprotonated hydroxyl group and oxygen of the carboxylic group of naphthoic acid moiety. Pd(II) forms mononuclear complexes (1:1) (M:L) with the two L^1 and L^2 azo dyes, Figure 10.

The thermodynamic parameters of the main thermal degradation steps (decomposition of the organic part of the complex) were calculated using Coats-Redfern equation. The relative thermal stability as reflected from the average value of the activation energies of the chelates is in the order Zn(II)- L^1 > Pd(II)- L^1 > Ni(II)- L^1 > Cu(II)- L^1 . The average of ΔS^* values of the decomposition stages for the complexes were found to be negative. The negative entropies of activation of complexes indicated that the studied complexes are in more ordered state and the decomposition reactions proceed with a much slower rate than the normal. The positive sign of ΔG^* suggests that the thermal decomposition steps are non-spontaneous process.

NiO and CuO nanoparticles which prepared from the thermal decomposition of Ni(II)- L^1 and Cu(II)- L^1 complexes at 600 °C have been characterized by X-ray diffraction (XRD), scanning electron microscopy (SEM) and Fourier transform infrared spectroscopy (FTIR). The results show that NiO and CuO nanoparticles can be prepared using Ni(II)- L^1 and Cu(II)- L^1 complexes with high purity.

The azo dyes and their complexes have been screened for their antibacterial activity against *Escherichia coli* as gram negative and *Staphylococcus aureus* as gram positive bacteria. The results of these study show that L^1 , Zn(II)- L^1 and Zn(II)- L^2 compounds are most active as antibacterial agent against *Staphylococcus aureus* and *Escherichia coli*.

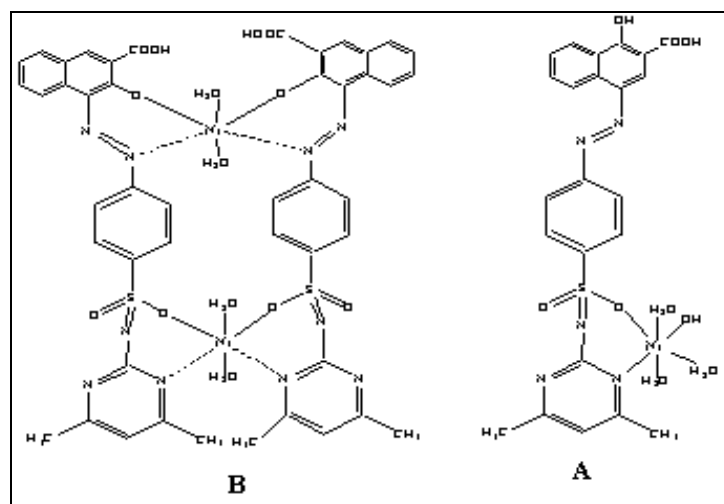


Figure 7: Structures of Ni(II)- L^1 (A) and Ni(II)- L^2 (B) complexes.

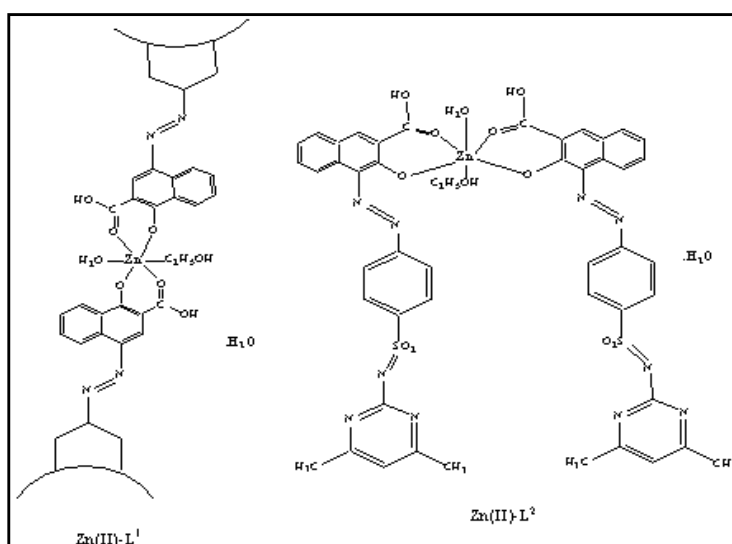


Figure 8: The structures of Cu(II) complexes.

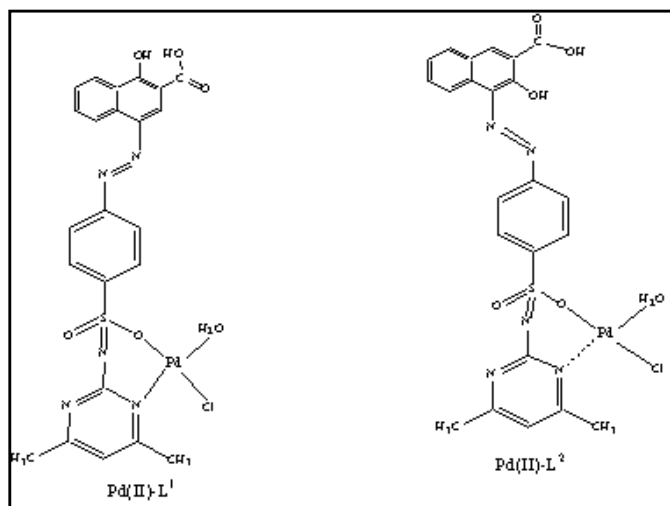


Figure 9: The structures of Zn(II) complexes.

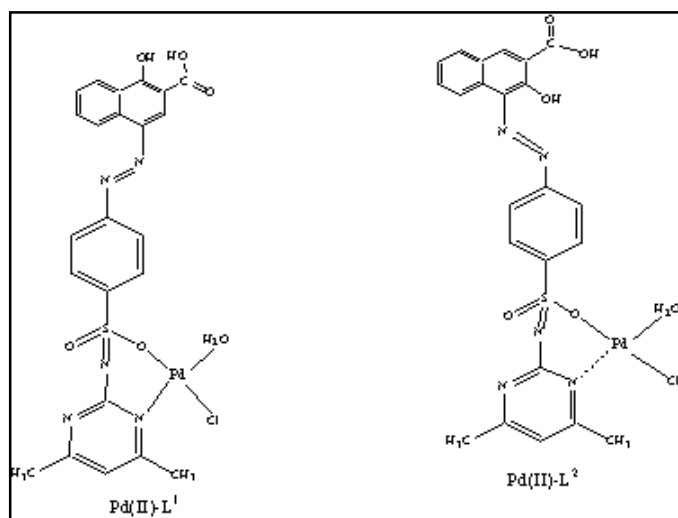


Figure 10: The structures of Pd(II) complexes.

5. References

- i. C. Sahoo, A. K. Gupta, and A. Pal, *Desalination*, 181(1-3), 91 (2005).
- ii. H. Kocaokutgen and S. Ozkinlt, *Dyes and Pigments*, 63 83 (2004).
- iii. K.C. Teo, *J. Chem. Analyst*, 126, 534 (2001).
- iv. A.E.Visser, R.P. Swatloski, S.T. Griffin, D.H. Hartman, R.D. Rogers, *Sep. Sci. Technol.*, 36, 785 (2001).
- v. L.S.G. Teixeira, F.R.P. Rocha, M. Korn, B.F. Reis, S.L.G. Ferreira and A.C.S. Costa, *Talanta*, 51, 1027 (2000).
- vi. AM. Khedr, M. Gaber, RM. Issa and H. Erten, *Dyes and Pigments*, 2, 117 (2005).
- vii. H. Song, K. Chen, D. Wu and H. Tian, *Dyes and Pigments*, 60, 111 (2004).
- viii. J. Nan, R. Brad and M. Andrew, *Org. Lett.*, 6, 4551 (2004).
- ix. D. Joshi and T.K. Joshi, *E. J. Chem.*, 1, 110 (2004).
- x. G. Valarmathy and R. Subbalakshmi, *Int J Pharm Bio Sci*, 4(2), 1019 (2013).
- xi. N. Mosconi, C. Giulidori, F. Velluti, E. Hure, A. Postigo, G. Borthagaray, D. Back, M. Torre and M. Rizzotto, *ChemMedChem*, 9, 1211 (2014).
- xii. E. El-Mossalamy, *Port. Electrochim. Acta*, 27, 143 (2009).
- xiii. A. Morsali, H. Monfared and A. Morsali, *Inorg. Chim. Acta.*, 362, 3427 (2009).
- xiv. Y. Mu, J. Yang, S. Han, H. Hou and Y. Fan, *Mater. Lett.*, 64, 1287 (2010).
- xv. K. Suslick, S. Choe, A. Cichowlas and M. Grinstaff, *Nature*, 353, 414 (1991).
- xvi. A. Aslani, A. Morsali, V. Yilmaz and C. Kazak, *Mol. Struct.*, 929, 187 (2009).
- xvii. A. Vogel, A.R. Tatchell, B.S. Furnis, J.A. Hannaford and P.W.G. Smith. *Vogel's Textbook of Practical Organic Chemistry*, fifth ed., Longmans, London (1989).
- xviii. A.M.G. Macdonald, P. Sirichanya, *Microchem. J.*, 14, 199 (1969).
- xix. A. W. Bauer, W. M. Kirby, C. Sherris and M. Turck, *American J. Clinical Pathology*, 45, 493 (1966).
- xx. National Committee for Clinical Laboratories standards, 1997, Performance vol. 41, 1997 antimicrobial susceptibility of Flavobacteria.

- xxi. National Committee for Clinical Laboratories standards, 1993. Methods for dilution antimicrobial susceptibility tests for bacteria that grow aerobically. Approved standard M7-A3. National Committee for Clinical Laboratories standards, Villanova, Pa.
- xxii. B. C. Rudy and B. Z. Senkowski, *Anal. Profiles Drug Subs.*, 2, 467 (1973).
- xxiii. Y. Pang, P. Xing, X. Geng, Y. Yang, F. Liu and L. Wang, *RSC Advances*, DOI: 10.1039/C5RA03837E.
- xxiv. W. J. Geary, *Coord. Chem. Rev.*, 7, 81 (1971).
- xxv. S. F. A. Kettle, *Coordination compounds*. Thomas Nelson and sons, London, 165 (1975).
- xxvi. A.A. Adel, A.A. Emara, A.A. Azza, *Spectrochim. A*, 64, 1010 (2006).
- xxvii. K. B. Pandeya and R. P. Singh, *J. Indian Chem. Soc.*, 60, 531 (1983).
- xxviii. D. Nicholls, *The Chemistry of Iron, Cobalt and Nickel*, 1st ed., Pergamon Press, Oxford, England.
- xxix. A. B. P. Lever, *Inorganic Electronic Spectroscopy*, Elsevier, Amsterdam, 1984.
- xxx. L. Larabi, Y. Hared, A. Reguig and M. Mostafa, *J. Serb. Chem. Soc.*, 68, 85 (2003).
- xxxi. A.E.M.M. Ramadan, M.M. Ibrahim and S.Y. Shaban, *J. Mol. Struct.*, 1006 (1), 348 (2011).
- xxxii. B. S. Manhas, *Indian J. Chem.*, 46A, 1226 (2007).
- xxxiii. Z.H. Chohan and H. Parvez, *Synth. React. Inorg. Met. Org. Chem.*, 23, 1061 (1993).
- xxxiv. M. Sekerci and E. Tas, *Heteroatom Chem.*, 11(4), 254 (2000).
- xxxv. S. Singh, N. Bharti, F. Naqvi, and A. Azam, *European Journal of Medicinal Chemistry*, 39, 459 (2004).
- xxxvi. S. Chandra, S. Raizada, and S. Rani, *Spectrochimica Acta A*, 71, 720.
- xxxvii. J. D. Lee "Concise Inorganic chemistry" 5th ed., Blackwell science publishers 967 (1999).
- xxxviii. B. Garcia, A. M. Lozano-vila, F. Luna-Giles, R. Pedreno-marin, *Polyhedron*, 25, 1399 (2006).
- xxxix. G. Speie, J. Csihony, A. M. Whalen and C. G. Pie-Ponti, *Inorg. Chem.*, 35, 3519 (1996).
- xl. D. Kivelson and R. Neiman, *J. Chem. Phys.*, 35, 149 (1961).
- xli. N.M. El-Metwally, I.M. Gabr, A.M. Shallaby and A.A. El-Asmy, *J. Coord. Chem.*, 58, 1145 (2005).
- xlii. G. Speier, J. Csihony, A.M. Whalen and C.G. Pierpont, *Inorg. Chem.*, 35, 3519 (1996).
- xliiii. U. Sagakuchi and A. W. Addison, *J. Chem. Soc. Dalton Trans.*, 660 (1979).
- xliv. K.Y. El-Baredie, *Monatsh. Chemie.*, 136, 1139 (2005).
- xlv. A. Coats and J. Redfern, *Kinetic parameters from thermogravimetric data*, 364 (1964).
- xlvi. M. Ahamed, H. Alhadlaq, M. A. Majeed Khan, P. Karuppiah and N. Al-Dhabi, *Journal of Nanomaterials*, 2014 (2014), ID 637858.
- xlvii. K. Anandan and V. Rajendran, *Mater. Sci. Semicond. Process*, 14, 43 (2011).
- xlviii. C.N.R. Rao, *chemical application of infrared spectroscopy*, Academic press, New York and London, (1963).
- xlix. I. Markova-Deneva, *J. Univ. Chem. Tech. Metal*, 45, 35 (2010).